Published in final edited form as:

Nat Med. 2017 July ; 23(7): 829–838. doi:10.1038/nm.4346.

Thermoneutral housing exacerbates non-alcoholic fatty liver disease in mice and allows for sex-independent disease modeling

Daniel A Giles[1,2], **Maria E Moreno-Fernandez**[1], **Traci E Stankiewicz**[1], **Simon Graspeuntner**[3], **Monica Cappelletti**[1], **David Wu**[4], **Rajib Mukherjee**[1], **Calvin C Chan**[1,2], **Matthew J Lawson**[1], **Jared Klarquist**[1,2], **Annika Sünderhauf**[5], **Samir Softic**[6], **C Ronald Kahn**[6], **Kerstin Stemmer**[7], **Yoichiro Iwakura**[8], **Bruce J Aronow**[9], **Rebekah Karns**[10], **Kris A Steinbrecher**[10], **Christopher L Karp**[11], **Rachel Sheridan**[12], **Shiva K Shanmukhappa**[12], **Damien Reynaud**[13], **David B Haslam**[14], **Christian Sina**[5], **Jan Rupp**[3], **Simon P Hogan**[4], and **Senad Divanovic**[1]

[1]Department of Pediatrics, Division of Immunobiology, Cincinnati Children's Hospital Research Foundation and the University of Cincinnati College of Medicine, Cincinnati, OH, USA

[2]Immunology Graduate Program, Cincinnati Children's Hospital Medical Center and the University of Cincinnati College of Medicine, Cincinnati, OH USA

[3]Department of Infectious Diseases and Microbiology, University of Lübeck, Lübeck, Germany

[4]Division of Allergy and Immunology, Cincinnati Children's Hospital Research Foundation and the University of Cincinnati College of Medicine, Cincinnati, OH, USA

[5]Institute of Nutritional Medicine, University Hospital Schleswig-Holstein, Campus Lübeck, Germany

[6]Section on Integrative Physiology and Metabolism, Joslin Diabetes Center, Boston, MA, USA

[7]Institute for Diabetes and Obesity, Helmholtz Diabetes Center & German Center for Diabetes Research (DZD), Helmholtz Zentrum München, Neuherberg, Germany

[8]Research Institute for Biomedical Sciences, Tokyo University of Science, Noda, Chiba, Japan

[9]Division of Biomedical Informatics, Cincinnati Children's Hospital Research Foundation and the University of Cincinnati College of Medicine, Cincinnati, OH, USA

[10]Division of Gastroenterology Hepatology and Nutrition, Cincinnati Children's Hospital Research Foundation and the University of Cincinnati College of Medicine, Cincinnati, OH, USA

*Correspondence: Senad Divanovic, Division of Immunobiology, Cincinnati Children's Hospital Research Foundation, TCHRF - Location S, Room #S.5.409, 3333 Burnet Avenue, Cincinnati, Ohio 45229-3039, U.S.A., Phone: 513-636-0286, Fax: 513-636-5355, senad.divanovic@cchmc.org.

Competing financial interests

The authors declare no competing financial interests.

Authors contributions

DAG, MEM-F, TES, SG, MC, DW, RM, CCC, MJL, JK, AS and DR participated in data generation. DAG, MEM-F, SG, DR, RK, SKS, RS, KAS, DBH, JR, SPH and SD participated in data analysis and interpretation. SS, KS, YI, CRK, BJA, CS and CLK provided materials and technical support and participated in critical review of the manuscript. DAG and SD participated in the conception and design of the study, obtained the funding and wrote the manuscript.

[11]Bill & Melinda Gates Foundation, Seattle, WA, USA

[12]Division of Pathology and Laboratory Medicine, Cincinnati Children's Hospital Research Foundation and the University of Cincinnati College of Medicine, Cincinnati, OH, USA

[13]Division of Experimental Hematology and Cancer Biology, Cincinnati Children's Hospital Research Foundation and the University of Cincinnati College of Medicine, Cincinnati, OH, USA

[14]Division of Infectious Diseases, Cincinnati Children's Hospital Research Foundation and the University of Cincinnati College of Medicine, Cincinnati, OH, USA

Abstract

Non-alcoholic fatty liver disease (NAFLD), a common prelude to cirrhosis and hepatocellular carcinoma, is the most common chronic liver disease worldwide. Defining the molecular mechanisms underlying the pathogenesis of NAFLD has been hampered by a lack of animal models that closely recapitulate the severe end of the human disease spectrum, including bridging hepatic fibrosis. Here, we demonstrate that a novel experimental model employing thermoneutral housing, as opposed to standard housing, resulted in lower stress-driven production of corticosterone, augmented mouse proinflammatory immune responses and markedly exacerbated high fat diet (HFD)-induced NAFLD pathogenesis. Disease exacerbation at thermoneutrality was conserved across multiple mouse strains and was associated with augmented intestinal permeability, an altered microbiome and activation of inflammatory pathways associated with human disease. Depletion of Gram-negative microbiota, hematopoietic cell deletion of Toll-like receptor 4 (TLR4) and inactivation of the interleukin-17 (IL-17) axis resulted in altered immune responsiveness and protection from thermoneutral housing-driven NAFLD amplification. Finally, female mice, typically resistant to HFD-induced obesity and NAFLD, develop full-blown disease at thermoneutrality. Thus, thermoneutral housing provides a sex-independent model of exacerbated NAFLD in mice and represents a novel approach for interrogation of the cellular and molecular mechanisms underlying disease pathogenesis.

Introduction

NAFLD, a leading precursor of hepatocellular carcinoma (HCC) and liver transplantation[1,2], encompasses a disease spectrum ranging from benign steatosis to nonalcoholic steatohepatitis (NASH) to cirrhosis[3]. Despite the clinical and public health significance, few effective therapies exist. Experimental and clinical evidence[4] suggests a complex interplay of multiple biological processes in disease development, including obesity, dysbiosis of the intestinal microbiome[5,6], heightened intestinal barrier permeability[7], metabolic endotoxemia and various inflammatory processes[5]. Notably, the combination of HFD feeding, intestinal microbiome dysbiosis, augmented intestinal permeability and metabolic endotoxemia/bacterial endotoxin (lipopolysaccharide; LPS) recognition all contribute to activation of both innate and adaptive immune responses central to the pathogenesis of NAFLD[5].

TLR4 polymorphisms and elevated hepatic TLR4 expression have been associated with human NAFLD[8,9]. In addition to innate immune system activation, TLR4 signaling also modulates multiple adaptive immune effector functions, including IL-17 axis activation[10].

Notably, IL-17 levels correlate with obesity and NAFLD progression in mouse models[11], and the transition from steatosis to NASH in humans is associated with hepatic infiltration of IL-17 producing cells[12]. Inactivation of the IL-17 axis inhibits progression from steatosis to NASH in mouse models[11]. However, while existing mouse NAFLD models employing both genetic (leptin deficiency) and dietary interventions (high fat, carbohydrate and/or cholesterol diets) have proven informative, a closer recapitulation of parameters relevant to human disease is still desired. Specifically, mouse NAFLD models are associated with a sex bias and limited progression to bridging hepatic fibrosis—something not observed in human NAFLD. These limitations, and the overall lack of representative animal models for preclinical testing, may be contributing to the paucity of therapeutic approaches for NAFLD[13].

The temperature at which mice are typically housed in research laboratories is associated with chronic cold stress that dramatically alters mouse physiology and immune responses[14]. The thermoneutral zone (T_N), or temperature of metabolic homeostasis, for *Mus musculus* is 30–32°C[15]. However, the standard temperature (T_S) range that mice are usually housed is between 20–23°C, a range chosen primarily for human comfort[14]. Housing mice at T_S, as opposed to T_N, conditions leads to remarkable physiological changes, including a heart rate increase of over 200 beats per minute, a 30% increase in mean arterial blood pressure[16], an overall increase in energy expenditure (50–60%)[16,17] and sustained upregulation of catecholamine and corticosteroid production[18]. Alleviating cold stress, through T_N housing, alters immune function in a variety of mouse models, including basal cytokine production[19], responses to bacterial[20] and viral[21,22] infection and tumor immunity[14,23]. Further, mice housed at T_S fail to develop fever after LPS challenge, while T_N housing promotes febrile responses following LPS challenge[20]. In context of metabolic diseases, T_N housing is required for modeling obesity in nude mice[17], exacerbates adipose tissue inflammation[24] and induces atherosclerosis in C57BL/6 WT mice[19]. Importantly atherosclerosis, the number one cause of mortality in NAFLD patients[25], is a disease poorly modeled in WT mice.

The relevance of T_N housing to the modeling of human disease is emerging. The majority of people in developed nations, where obesity is classified as a disease, tend to spend most of their day within their thermoneutral zone via utility of climate control inside their dwellings. Further, exposure to non-thermoneutral conditions, profoundly impacts both immune response and metabolic disease in humans. Specifically, exposure to sustained cold stress leads to a dampened immune responsiveness to LPS challenge[26], and improves glucose tolerance in type 2 diabetics[27]. Thus, given its role in both metabolism and inflammation, we hypothesized that T_N housing would allow for development of an improved, exacerbated and more “human-like” mouse model of NAFLD.

T_N housing alters BAT function and immune responsiveness

Adaptation to cold stress involves, among other things, heightened brown adipose tissue (BAT) activity, energy expenditure and glucocorticoid production[28]. Compared to the mild cold stress associated with T_S (22°C) housing, wild-type (WT) C57BL/6 mice at T_N (30°C) resulted in lower total body energy expenditure[29] and expression of genes central to BAT activity, including glucocorticoid receptor (GR; *N3cr1*), beta 3 adrenergic receptor (β3AR;

Adrb3; catecholamine receptor), peroxisome proliferator-activated receptor gamma coactivator 1 alpha (*Ppargc1a*) and uncoupling protein 1 (*Ucp1*) (Fig. 1a). Further, compared to T_S housing, T_N housing resulted in lower serum concentrations of corticosterone (an immunosuppressive glucocorticoid[30]) and splenic expression of genes known to inhibit inflammatory responses including, GR, beta 2 adrenergic receptor (β2AR; *Adrb2*; catecholamine receptor), *Ppargc1a*, and uncoupling protein 2 (*Ucp2*)[31] (Fig. 1b,c). Notably, immune cells deficient in GR, β2AR or UCP-2 exhibit exacerbated proinflammatory cytokine production following LPS stimulation[32–34]. These effects were not unique to splenic cells, as an unbiased approach employing RNA sequencing of peripheral blood mononuclear cells (PBMCs) revealed that T_S housing, compared to T_N, resulted in greater levels of gene expression in pathways known to negatively regulate the immune responses, including pathways responsible for decreased inflammatory responses, increased susceptibility to infection, and decreased acute inflammation (Fig. 1d and Supplementary Table 1a).

We next examined the functional relevance of altered immune gene expression observed with differences in housing temperature on proinflammatory cytokine production. *In vivo* analysis revealed that T_N, compared to T_S, housing exacerbated systemic TNF and IL-6 levels at baseline and after LPS challenge (Fig. 1e). These effects persisted *ex vivo*, as LPS stimulation of splenocytes and bone marrow-derived dendritic cells (BMDCs) from T_N-housed, as compared to T_S-housed, mice resulted in heightened TNF and IL-6 production (Fig. 1f). Changes observed at T_N, compared to T_S, were found to be independent of alterations in bone marrow, PBMC, spleen and thymus cellularity and composition (Supplementary Fig. 1a–d). These findings indicate T_N housing reverses the inhibition of immune responsiveness seen under standard housing conditions.

The anti-inflammatory effects of glucocorticoids and corticosterone are well established. We thus examined the relevance of the corticosterone axis on immune responsiveness at T_N. Administration of corticosterone to T_N-housed mice was sufficient to reverse the exacerbated proinflammatory cytokine production associated with T_N, as compared to T_S, housing (Fig. 1g), suggesting that the corticosterone axis is functional at T_N and plays a role in regulation of inflammatory vigor. Conserved effects were observed in humans following stimulation of human PBMCs with LPS in the presence of GR and β2AR agonists (data not shown)[35]. In sum, these results suggest that ambient temperature profoundly alters BAT function, glucocorticoid production and the host innate immune responses in male C57BL/6 mice, and are congruent with reports indicating that T_N housing promotes a more “human-like” immune response[20].

T_N housing exacerbates HFD-driven NAFLD pathogenesis

As the immune system plays a central role in the pathogenesis of obesity-associated sequelae, we hypothesized that T_N housing, compared to T_S housing, would exacerbate such effects in male, C57BL/6 WT mice. T_N housing combined with HFD feeding initially accelerated weight gain compared to T_S-housed HFD-fed animals, however prolonged dietary exposure nullified differences in weight gain, body lean or fat mass (Fig. 2a,b). Similar weight gain occurred despite a lower extent of food intake at T_N (Fig. 2c), likely due

to lower energy expenditure at T_N[16,17]. However, despite similar body weight and adiposity, at the time of harvest, T_N-housed mice displayed heightened visceral adipose tissue immune cell infiltration and adipose tissue macrophage activation, compared to T_S-housed, HFD-fed mice (Supplementary Fig. 2a–c)—in agreement with a previous report[24].

Given the role of obesity and adipose tissue inflammation in glucose dysmetabolism[36] we next evaluated the impact of T_N housing on glucose homeostasis. T_N housing, compared to T_S, exacerbated glucose intolerance only when differences in body weights existed (Supplementary Fig. 2d). These differences in glucose tolerance diminished once body weights were normalized (Supplementary Fig. 2e). Further, with similar weight gain, both T_N and T_S mice displayed similar insulin sensitivity (Supplementary Fig. 2f) which correlated with similar islet sizes and hepatic levels of AKT phosphorylation (data not shown). These data agree with previous reports describing the role of T_N housing in modulation of glucose metabolism and insulin resistance in obesity[24].

The impact of T_N housing on NAFLD development and progression was examined next. Despite similar serum triglyceride and serum and hepatic cholesterol levels (Supplementary Fig. 2g–i), T_N-housed, compared to T_S-housed, obese mice had exacerbated liver weight and hepatic steatosis as quantified by hepatic triglyceride levels, Oil Red O staining and NAFLD activity score[37] (Fig. 2d–h). Histological analysis, used to quantify NAFLD activity score, suggested that hepatocytes from T_N-housed, as compared to T_S-housed, obese mice exhibited elevated steatosis, and hepatocyte ballooning characterized by cellular swelling, rarefaction of the hepatocytic cytoplasm and clumped strands of intermediate filaments (Fig. 2g). These findings also correlated with lower gene expression of key lipid mediators known to be reduced during NASH (Fig. 2i)[38,39].

Progression to, and the severity of, NASH under T_N housing was examined next. Modest changes in expression of genes related to lipid handling, chemokine production and fibrosis were observed in mice fed a chow diet (Supplementary Fig. 3a–c). In the context of HFD feeding, however, T_N-housed mice exhibited robust exacerbation of hepatic chemokine expression (Fig. 2j)[3], macrophage infiltration (Fig. 2k), and bacterial translocation to the liver, compared to T_S-housed mice (Fig. 2l). Further, T_N-housed, as compared to T_S-housed, obese mice, also displayed elevated expression of genes associated with hepatic fibrosis induction (Fig. 2m) and a 3-fold induction in hepatocellular damage as measured by serum alanine transaminase (ALT) levels (Fig. 2n). However, despite such robust changes, the induction of overt bridging hepatic fibrosis was not observed in WT C57BL/6 mice (Supplementary Fig. 3d).

To begin to examine the effect of T_N housing on hepatic gene expression in the presence or absence of dietary modulation, an unbiased approach utilizing RNASeq analysis of liver tissue was performed. Although T_N, compared to T_S housing, altered hepatic gene expression in chow fed mice, exposure to HFD exacerbated differential gene expression (Supplementary Fig. 3e). In chow fed mice, analysis of differential gene expression revealed alterations in liver metabolism, including elevated expression of gene pathways associated with lipid metabolism and fatty acid oxidation (Supplementary Fig. 3e,f and Supplementary Table 1b). In contrast, analysis of differential gene expression in HFD-fed mice revealed

heightened expression of genes and gene pathways associated with collagen formation, apoptosis and HCC induction (Fig. 2o and Supplementary Table 1c). Further, comparison of hepatic gene expression changes induced by T_N versus T_S housing on HFD to known gene expression changes induced by human NASH[40], revealed that T_N drove similar changes in expression of genes associated with a variety of NAFLD-related pathways (*e.g.,* Inflammatory response, Response to reactive oxygen species and Leukocyte activation; Supplementary Fig. 3g).

Next, we compared whether changes in HFD-induced hepatic gene expression at T_N or T_S are more likely to predict gene expression patterns induced by human NASH[40]. Utility of support vector machine analysis[41] determined that the gene expression differences induced by HFD feeding at T_N allowed for an improved prediction of human NASH, over T_S housing and HFD (Fig. 2p). These findings verify markedly exacerbated HFD-driven NAFLD pathogenesis and hepatocellular damage at T_N and suggest an improved model for human disease.

Although most commonly used for obesity and NAFLD modeling, the C57BL/6 mouse strain is highly resistant to induction of hepatic fibrosis. Thus, we next determined if the lack of overt hepatic fibrosis observed in C57BL/6 mice was strain specific. Notably, the AKR strain of mice develop robust obesity and NAFLD when fed a HFD[42]. When housed at T_N, as opposed to T_S, and fed a HFD, AKR mice gained more weight but maintained similar visceral and subcutaneous adiposity (Supplementary Fig. 4a,b). T_N-housed, obese AKR mice exhibited greater liver weight, hepatic steatosis, and NAFLD activity scores compared to T_S-housed AKR controls (Supplementary Fig. 4c–f). The lower NAFLD activity scores observed in AKR mice, compared to C57BL/6 mice, may be mouse strain dependent and/or due to shortened HFD exposure. The NAFLD activity score in AKR mice was associated with greater lobular inflammation and steatosis at T_N, but limited hepatocyte ballooning was observed in either group at this time. This correlated with higher hepatic chemokine gene expression, macrophage infiltration, and hepatocellular damage (Supplementary Fig. 4g–i) in T_N-housed, compared to T_S-housed, AKR mice. Importantly, unlike in C57BL/6 mice, HFD feeding under conditions of T_N housing, but not T_S housing, was sufficient to induce fibrosis in AKR mice, as quantified by hepatic gene expression and Trichrome staining (Supplementary Fig. 4j–k). Together, these data indicate that the effects of T_N housing on NAFLD pathogenesis are conserved across different mouse strains, and suggest that the use of obese AKR mice at T_N may provide a novel and accelerated model for mechanistic interrogation of NAFLD-induced hepatic fibrosis.

Adrenal glands are a central production site of circulating corticosterone and catecholamines. Immune responsiveness under cold stress is, in part, modulated by corticosterone and catecholamine levels. C57BL/6 adrenalectomized male mice fed a HFD exhibited similar weight gain and visceral and subcutaneous adiposity at either housing temperature (Supplementary Fig. 5a–d). Unlike C57BL/6 mice with intact adrenal glands, adrenalectomized C57BL/6 mice housed at T_N or T_S exhibited similar liver weights, hepatic steatosis, lipid handling and chemokine gene expression, macrophage infiltration, expression of genes associated with induction of fibrosis and hepatocellular damage (Supplementary Fig. 5e–l). Notably, the lack of adrenal glands at T_S housing, in combination with HFD,

exacerbated hepatocellular damage compared to non-adrenalectomized mice at T_S and resulted in levels similar to those observed in T_N-housed mice (Supplementary Fig. 5m). These data suggest that mediators produced by the adrenal glands play an important role in suppressing NAFLD progression during cold stress.

Intestinal permeability and microbiome in T_N-driven NAFLD

Augmented intestinal permeability[7] and dysbiosis of the intestinal microbiome[6] contribute to human and mouse NAFLD progression[4–6]. Although, histological analysis of the small intestine revealed no housing temperature or diet driven differences in immune cell infiltration (Supplementary Fig. 6a), T_N housing, compared to T_S, exacerbated para-cellular intestinal permeability, as evidenced by translocation of FITC-dextran across the epithelium, and lowered trans-epithelial resistance on both chow and HFD (Fig. 3a and Supplementary Fig. 6b). Further, T_N housing, compared to T_S housing, changed intestinal microbiome in as little as 2 weeks, prior to being placed on HFD (Supplementary Fig. 6c,d). Extended exposure (12 weeks) of randomly separated WT C57BL/6 mice to differential ambient temperatures or HFD further exacerbated these differences, with obvious differences observed in every phyla analyzed after 24 weeks of exposure (Fig. 3b and Supplementary Figs. 6e–k). Notably, T_N housing enriched the representation of Bacteroidetes, while T_S housing preferentially enriched for Firmicutes. Linear discriminant analysis effect size (LEfSe) analysis, which was employed to analyze data with specificity to the genus level, revealed congruent differences beyond the phylum level (Supplementary Fig. 7).

While the microbiome plays a role in NAFLD in both humans and mice, the two species display an inherently different microbial composition. Nevertheless, we examined whether the mouse microbiome at T_N correlated more closely with microbiomes reported in NASH patients[6]. Comparison of 16S rRNA sequences demonstrated that T_N housing of mice on a HFD led to greater similarity of their gut microbiome to that observed in patients with NASH[6]. Notably, this was seen in both phyla level alterations (Fig. 3c) and principle component analysis (Fig. 3d), where an upward shift (PC2) corresponds with a more NASH-like metagenome.

T_N housing in combination with HFD stress promoted expansion of Gram-negative Bacteriodetes (Fig. 3b). Antibiotic-mediated depletion of the Gram-negative microbiome in HFD-fed mice housed at T_S and T_N, did not alter total body weight gain, visceral and subcutaneous adiposity, hepatic weight or hepatic triglyceride accumulation, although T_S-housed, antibiotic-treated mice displayed elevated glucose intolerance (Supplementary Fig. 8a–g). However, antibiotic treatment obviated the greater intestinal permeability observed in HFD fed mice housed at T_N, compared to Ts (Fig. 3e), lowered NAFLD activity inflammation score (Fig. 3f,g), and protected from hepatocellular damage only at T_N (Fig. 3h). Of note, these protective effects in NAFLD were specific to obese T_N-housed mice and were not observed in obese, antibiotic-treated, T_S-housed mice (Fig. 3f–h and Supplementary Fig. 8g). These data indicate that changes in intestinal microbiome composition are associated with T_N-driven amplification of NAFLD.

Hematopoietic TLR4 and IL-17 axis in T_N-driven NAFLD

LPS from Gram-negative bacteria activates TLR4. Our data indicate that TLR4 responsiveness is elevated at thermoneutrality (Fig. 1e,f). Additionally, TLR4 polymorphisms and TLR4 expression have been correlated with the progression of human NAFLD[9]. Whether T_N-driven modulation of innate immune responses is maintained on HFD has not been examined. RNASeq analysis of PBMCs from WT, C57BL/6 mice challenged with HFD, revealed greater levels of gene expression in pathways associated with cytokine production and TLR responsiveness (Fig. 4a and Supplementary Table 1d). To determine the functional relevance of differential immune cell TLR4 expression, $TLR4^{fl/fl}$ mice were utilized. Congruent with a previous report[43], Vav1-Cre-driven hematopoietic cell deletion of TLR4 in T_S-housed mice did not hinder the progression of HFD-induced NAFLD (Fig. 4b–d). However, under T_N housing, such deletion was sufficient to protect from HFD-driven increases in weight gain, visceral and subcutaneous adiposity, glucose intolerance, liver weight, histologically identifiable steatosis, hepatocyte ballooning and lobular inflammation and hepatocellular damage (Fig. 4b–d and Supplementary Fig. 9). These data indicate that TLR4 signaling is fundamentally modulated by ambient temperature in the context of HFD feeding, and that removing suppression of TLR4 signaling through T_N housing can contribute to NAFLD pathogenesis.

Induction of IL-6, IL-1β and IL-23 production is associated with Th17 cell polarization and IL-17 axis activation[10]. Hepatic IL-6 expression is elevated in human NAFLD, and serum concentrations of IL-1β levels are higher in patients with metabolic syndrome[44,45]. RNAseq analysis of PBMCs from WT C57BL/6 mice provided initial suggestions that T_N housing, compared to T_S housing, coupled with HFD resulted in greater expression of genes related to IL-17 production (Fig. 5a and Supplementary Table 1d). We next examined whether T_N housing altered TLR4 signaling-driven induction of mediators associated with activation of the IL-17 axis. LPS stimulation of BMDCs from T_N-housed, compared to T_S-housed, obese mice resulted in greater IL-6, IL-1β production and *Il23a* gene expression (Supplementary Fig. 10a–c). Elevated production of these mediators correlated with exacerbated hepatic infiltration of $CD4^+$ T cells capable of both single $IL\text{-}17^+$ and dual $IL\text{-}17^+/TNF^+$ production, in T_N-housed, obese mice (Fig. 5b,c). Notably, dual $IL\text{-}17^+/TNF^+$ producing $CD4^+$ T cells exacerbate pathogenesis in mouse experimental autoimmune encephalomyelitis models[46] and have been associated with higher severity of Crohn's disease in humans[46,47]. Hence, the contribution of IL-17 axis activation to T_N-driven NAFLD pathogenesis was examined. Despite similar weight gain, visceral and subcutaneous adiposity, hepatic steatosis, and NAFLD activity score analysis (Fig. 5d,e and Supplementary Fig. 10d–h), T_N-housed, obese, IL-17 axis-deficient mice ($IL\text{-}17RA^{-/-}$ and $IL\text{-}17A^{-/-}$) were protected from glucose intolerance, exacerbated liver weight and hepatocellular damage, compared to T_N-housed WT controls (Fig. 5f and Supplementary Fig. 10i,j). These findings suggest that IL-17 axis is a relevant factor in regulation of NAFLD pathogenesis and that, unlike TLR4 signaling, a role for IL-17 axis in NAFLD is conserved across housing temperatures.

Serum amyloid A (SAA), an acute phase protein produced largely in the liver, is known to both activate TLR4 and promote Th17 cell differentiation via antigen presenting cells[48]. T_N-housed, obese mice exhibited greater hepatic SAA 1 and 2 expression, compared to T_S-

housed mice (Supplementary Fig. 11a), while deletion of IL-17RA, IL-17A or hematopoietic TLR4 was associated with lower hepatic expression of SAA1 (Supplementary Fig. 11b,c). These data suggest that T_N-mediated modulation of SAA production might represent a link between the activation of the TLR4 and IL-17 axes.

T_N housing allows for disease modeling in female mice

Human NAFLD equally affects men and women[49]. However, protection from severe HFD-induced obesity and NAFLD in C57BL/6 female mice precludes the interrogation of disease pathogenesis in a sex-independent manner. Hence we asked whether T_N housing would allow for the induction of obesity and NAFLD in C57BL/6 female mice. As expected, T_S-housed female mice fed HFD, as compared to chow, displayed mild weight gain over time (Fig. 6a). However, T_N-housed female mice fed HFD, as compared to chow, exhibited robust obesity and total body adiposity (Fig. 6a,b)—to the levels observed in T_N-housed male mice (Fig. 2). Further, in agreement with data in male mice, under conditions of robust weight gain, obese, T_N-housed female mice displayed exacerbated glucose intolerance (Supplementary Fig. 12a).

Similarly, T_N-housed, obese female mice exhibited greater liver weight, hepatic steatosis, hepatic chemokine expression[3], macrophage infiltration, and hepatic infiltration of both single IL-17^+ and dual IL-17^+/TNF^+ producing Th17 cells, compared to T_S-housed, HFD-fed mice (Fig. 6c–i). Further, as in WT C57BL/6 male mice, these physiological changes in the liver correlated with greater expression of fibrosis-associated genes (*Acta2*, *Col1a1* and *Col1a2*) and a greater degree of hepatocellular damage (Fig. 6j,k) but did not induce overt bridging hepatic fibrosis (Supplementary Fig. 12b) in obese T_N-housed compared to T_S-housed female mice. Notably, T_N-housed, compared to T_S-housed, obese WT female mice exhibited greater SAA1 gene expression (Supplementary Fig. 12c). Thus, T_N housing allows for development of robust obesity and NAFLD in WT C57BL/6 female mice and, importantly, removes the sex bias typically associated with experimental modeling of mouse obesity and NAFLD. In sum, these findings demonstrate that T_N housing-driven NAFLD pathogenesis represents a novel disease model associated with altered corticosterone levels, immune responses, metabolism, intestinal barrier integrity and intestinal microbiome (Fig. 6l).

Discussion

NAFLD research often involves the use of mouse models housed at a suboptimal, cold stress-inducing, ambient temperature (typically 22°C) that fails to comprehensively recapitulate human disease. In the case of NAFLD, current models in mice include a fundamental sex bias, unlike in humans; an inability to study the interplay between atherosclerosis and NAFLD; limited induction of pathways associated with development of hepatic fibrosis and hepatocellular carcinoma; and altered immune responsiveness compared to humans with this condition. While previous reports have demonstrated that housing mice at a thermoneutral temperature (T_N; 30°C) affects the pathogenesis of multiple infectious and metabolic complications, whether T_N housing allows for an improved mouse NAFLD model has not been previously interrogated.

Here, we demonstrate, in accordance with previous reports, that the cold stress associated with standard mouse housing procedures inhibits immune responses[14]. Housing mice at T_N upregulated immune responsiveness both *in vivo* and *ex vivo*, something suppressed by exogenous administration of corticosterone. Further, T_N housing exacerbates cellular responsiveness to inflammatory ligands, without alteration of the cell type composition or numbers. Additional studies, however, are required to functionally examine the pathways central to altered immune cell responsiveness at T_N. As such changes are sustained *ex vivo*, T_N-driven modulation of cellular metabolism and epigenetics are likely to play a role and warrant further investigation.

Robust exacerbation of NAFLD pathogenesis in context of T_N housing and HFD-stress correlated with heightened hepatic steatosis, hepatic immune cell infiltration, elevated expression of genes associated with hepatic fibrosis and HCC, and hepatocellular damage. Therefore, T_N-driven amplification of disease-propagating processes may allow for in-depth interrogation and improved definition of mechanisms central to NAFLD pathogenesis, including critical sites of inflammation, cell type(s), and immune mediators, using a genetically unbiased approach. However, despite robust disease exacerbation hepatic fibrosis was not observed in male or female WT C57BL/6 mice. Thus, additional examination of hepatic fibrosis development in C57BL/6 mice, using T_N housing in combination with dietary challenges known to promote fibrosis (*e.g.*, methionine choline deficient diets, high fat plus high cholesterol and high fat plus high fructose diets)[50] might offer a clear advantage over existing experimental NAFLD models for evaluating novel therapeutics. Notably, the induction of measureable hepatic fibrosis by HFD at T_N is possible, as demonstrated in AKR mice. Employing these mice in future studies may provide a novel model for mechanistic interrogation of NAFLD-induced hepatic fibrosis. Lastly, T_N housing appears to hold relevance to human disease and improve upon existing NAFLD models, even in C57BL/6 mice, as hepatic gene expression in this model provides improved prediction of human NASH.

Interactions between the microbiome and the immune system are thought to play a key role in NAFLD. Augmented intestinal permeability also correlates with NASH severity[7]. Notably, T_N housing and HFD feeding resulted in heightened intestinal permeability and intestinal microbiome dysbiosis, which mirrors that observed with human obesity- and NASH-driven dysbiosis[6]. Intestinal microbiome changes are certainly one of the many factors in the causal nexus that allow pronounced expression of the NAFLD phenotype in mice housed at thermoneutrality. However, given the consistency in the impact of T_N housing in modulation of immune responses and metabolism among multiple research institutions, it is unlikely that a unique “microbiome mix”, specific to a single institution, is driving observed differences independent of temperature effects. Notably, our data evoke several interesting questions and areas of future study, including: What are the bidirectional interactions between altered microbiome and altered immune responsiveness under T_N housing? Does T_N housing alter the immune response in gnotobiotic mice? Can protection from HFD-driven obesity in germ-free mice[51] be reversed utilizing T_N housing? Are levels of specific microbial byproducts or microbial species thought to play a role in obesity-associated inflammation and NAFLD altered at T_N[11,52]?

Our data suggest that TLR4 signaling, presumably via Gram-negative microbiome dysbiosis, plays a role in T_N-driven NAFLD pathogenesis. Additionally, we demonstrate that this pathogenic role for Vav1-driven deletion of TLR4 expression is important only when mice are housed at T_N. Of note, Vav1-cre can be activated in different cells, and the necessary hematopoietic and/or endothelial cell type should be evaluated[53]. Also, whether TLR4's role is dependent on LPS or on induction of various endogenous TLR4 ligands (*e.g.,* HMGB1, fibronectin, fibrinogen and resistin) that have been associated with NAFLD progression[43,54–56] is unknown.

Our findings also highlight the functional effector relevance of the IL-17 axis in T_N-housing driven NAFLD. The cellular and molecular mechanisms underlying IL-17 mediated effects in NAFLD are not well defined. IL-17-driven induction of chemokines (*e.g.,* CXCL1 and CCL2) is associated with both macrophage and neutrophil hepatic infiltration and activation[57]. Further, IL-17 has been demonstrated to play a significant role in liver fibrosis[58]. Notably, both *Cxcl1* and *Ccl2* hepatic expression and markers of fibrosis are elevated in T_N-housed, HFD-fed livers. Thus, definition of the critical IL-17RA-expressing cell type(s) within the liver (*e.g.,* hepatocytes, stellate cells, Kupffer cells, etc.) deserves examination. Similarly, definition of the critical IL-17 producing cell type(s) requires additional characterization. Notably, while $CD4^+$ T cells are primary IL-17 producers, a variety of other cells, including $CD8^+$ T cells and innate lymphoid cells, have been shown to produce IL-17 within the liver[59].

Corticosterone levels are higher in mice housed at T_S. Our findings demonstrated that exogenous administration of corticosterone in T_N mice is sufficient to prevent augmented immune responsiveness. In contrast, adrenalectomy removes the inhibition of NAFLD pathogenesis associated with T_S, as compared to T_N, housing. These data suggest that specific signaling mediators released via the adrenal glands may play a suppressive role in NAFLD pathogenesis. Of note, chemical inhibition of β-adrenergic receptor signaling exacerbates NAFLD progression in mice[60]. However, β-adrenergic receptors also play a homeostatic role in intestinal, liver and immune cells. Thus, future studies employing the use of β2AR, β3AR and/or GR cell type specific knockouts are required to better define contribution of these pathways to NAFLD pathogenesis.

Human obesity and NAFLD are equally represented in males and females[49]. The ability of T_N housing to promote development of robust obesity and NAFLD in female mice further supports the relevance of T_N housing to human physiology and allows for the realization of novel pathways associated with protection from HFD-driven obesity in female mice. Importantly, T_N housing may allow for improved modeling of the contribution of maternal obesity on disease pathogenesis over generations of offspring. In addition, atherosclerosis, the most common cause of mortality in NAFLD patients[25], is another metabolic disease that lacks an appropriate mouse model that is similarly sex restrained. Importantly housing WT mice at T_N in combination with a "western" diet allows for atherosclerosis induction in male C57BL/6 mice[19] and hence might provide for interrogation of pathways critical for the interplay of these two diseases as well as for removing sex bias in modeling atherosclerosis.

Thus, housing temperature is an overlooked and very important variable in the modeling of human disease. Close attention to this variable has promise for discovery of novel mechanisms underlying disease pathogenesis and for improved modeling of the non-communicable metabolic diseases that are causing an increasing burden of morbidity and mortality worldwide.

Methods

Mice

With the exception of AKR mice (Jackson), all male and female mice used were on a C57BL/6 background. WT, TLR4$^{fl/fl}$ [61], IL-17RA$^{-/-}$ (Amgen)[11], and IL-17A$^{-/-}$ [62] mice were bred at Cincinnati Children's Hospital Medical Center (CCHMC) in a specific pathogen-free (spf) facility maintained at 22°C, with free access to autoclaved food (LAB Diet #5010; calories provided by carbohydrates [58%], fat [13%] and protein [29%]) and water. 6 week old adrenalectomized mice, on a C57BL/6 background, were obtained from Jackson. For experimental purposes, mice were randomly allocated to groups and housed in separate spf units contained within the same animal barrier but maintained at either 22°C or at 30–33°C. All care was provided in accordance with the Guide for the Care and Use of Laboratory Animals. All studies were approved by the CCHMC IACUC.

Corticosterone Levels

Serum corticosterone levels were detected by ELISA according to manufacturer's instructions (Arbor Assays).

qRT-PCR

Tissue samples were homogenized in TRIzol (Invitrogen), RNA was extracted, reverse transcribed to cDNA (Verso cDNA Synthesis Kit; Thermo Scientific) and subjected to qPCR analysis (Light Cycler 480 II; Roche) – all according to manufacturer's instruction as previously described[63]. The following primers pairs were used: *Nr3c1* For CCATAATGGCATACCGAAGC Rev AGGCCGCTCAGTGTTTTCTA – *Adbr2* For TAGCGATCCACTGCAATCAC Rev ATTTTGGCAACTTCTGGTGC – *Ppargc1a* For CTGCTAGCAAGTTTGCCTCA Rev AGTGGTGCAGTGACCAATCA – *Ucp1* For TCAGCTGTTCAAAGCACACA Rev GTACCAAGCTGTGCGATGTC – *Ucp2* For TCCTGCTACCTCCCAGAAGA Rev CTGAGACCTCAAAGCAGCCT – *Srebp1c* For CTGTCTCACCCCCAGCATAG Rev GATGTGCGAACTGGACACAG – *Ppara* For CATGGGGAGAGAGGACAGA Rev AGTTCGGGAACAAGACGTTG – *Col1a1* For GGTTTCCACGTCTCACCATT Rev ACATGTTCAGCTTTGTGGACC – *Col1a2* For AGCAGGTCCTTGGAAACCTT Rev AAGGAGTTTCATCTGGCCCT – *Ccl2* For AGATGCAGTTAACGCCCCAC Rev TGTCTGGACCCATTCCTTCTTG – *Ccl3* For ACCATGACACTCTGCAACCAAG Rev TTGGAGTCAGCGCAGATCTG – *Cxcl1* For ACCCAAACCGAAGTCATAGC Rev TCTCCGTTACTTGGGGACAC; *Il23a* For AGGCTCCCCTTTGAAGATGT Rev TTGTGACCCACAAGGACTCA – *Saa1* For CATTTGTTCACGAGGCTTTCC Rev GTTTTTCCAGTTAGCTTCCTTCATGT – *Saa2* For TGTGTATCCCACAAGGTTTCAGA Rev TTATTACCCTCTCCTCCTCAAGCA –Beta-actin (*Actb*) For GGCCCAGAGCAAGAGAGGTA Rev GGTTGGCCTTAGGTTTCAGG.

mRNA expression of each gene was compared to Beta-actin expression (endogenous house-keeping gene control).

RNA sequencing and gene expression quantification

PBMCs were collected from mice fed a chow or HFD for 8 weeks. Liver samples were collected from mice fed a chow or HFD for 24 weeks. Gene expression was determined by running 50 base pair single-end reads (~20 million reads per sample). All transcriptomic analyses were performed in StrandNGS. Following the removal of barcodes and primers, raw reads were aligned to the mm10 genome using annotations provided by UCSC with the following parameters: (1) minimum percent identify = 90; (2) maximum percent gaps = 5; (3) minimum aligned read length = 25; (4) number of matched to output per read = 1; and (5) ignore reads with more than 5 matches. The proprietary aligner (COBWeb) is based on the Burrow Wheeler Transform method. Aligned reads were used to compute reads per kilobase per million (RPKM) using the Expectation-Maximization algorithm for the maximum likelihood estimation of expression. Further, RPKM were thresholded at 1 and normalized using the DESeq algorithm, which computes a normalization factor (NF) for each sample. Within each sample, each transcript is divided by that transcript's geometric mean across samples. The within-sample median of these values is that sample's NF. To obtain normalized counts, a sample's raw RPKM are divided by that sample's NF. Finally, normalized per-transcript RPKM were baselined to the median of all samples. Reasonably expressed transcripts (raw RPKM >3 in 100% of samples in at least one condition) were included for differential analysis. Differential expression was determined through 2-Way ANOVAs with an FDR-corrected p-value cutoff of 0.05 and a fold change requirement of >2. Raw data can be accessed at GSE80976. For pathway analysis, the database at toppgene.cchmc.org was employed, which amasses ontological data from over 30 individual repositories[64].

We performed candidate gene prioritization on differentially regaled genes between T_N and T_S animals on HFD. Using the Toppgene Suite Candidate Prioritization tool, we ranked genes based on their functional similarity to NASH-related genes (extracted from the NASH-profiler; healthy obese v NASH at FDR-p-value<0.05 and FC>2). The top 20 ranked genes were submitted to ToppCluster and Cytoscape for ontological assessment and visualization (data depicted in Supplementary Fig. 3g).

Further, using a human NASH cohort, we assessed the ability of genes differentially regulated under HFD conditions compared to chow in T_S and T_N housing conditions to discriminate between healthy obese controls and individuals with NASH. Using Support Vector Machine (SVM), we quantified the discriminative capabilities of the following gene sets: 1) differentially regulated between HFD and Chow in T_N; 2) differentially regulated between HFD and Chow in T_S; and 3) differentially regulated genes between healthy obese controls and NASH identified through the NASH-profiler[40]. Model accuracy was compared between the three gene sets (data depicted in Fig. 2p).

Cytokine Production

Cytokines were detected employing biotinylated capture antibodies, detection antibodies and recombinant protein mouse standards. For *in vivo* production, *in vivo* cytokine capture assays were employed as previously described[11,65,66]. Briefly, cytokines were detected using IVCCA employing biotinylated capture antibodies [IL-6 (MP5-32C11), TNFα (TN3-19)] detection antibodies and recombinant protein mouse standards, all from eBioscience. Biotinylated capture antibodies were injected via tail vein or intraperitoneally and terminal serum collection was performed 24 hours later. For *in vitro* production, ELISAs were employed as previously described[11,65]. For mice, cytokine levels of TNF and IL-6 were determined according to manufacturer's protocol (BD OptEIA).

Cell culture and in vitro cytokine production

Mouse BMDCs were differentiated as previously described[67]. Mouse splenocytes and BMDCs were stimulated with ultrapure LPS (100 ng/mL; Invivogen) for 4 hours or with 1μM norepinephrine or dexamethasone as noted.

Obesity and NAFLD Model

At 6 weeks of age mice were randomly separated into T_S or T_N housing facilities. After 2 weeks of acclimation, mice were fed either an irradiated high fat diet (HFD; Research Diets #D12492; 60% of calories from fat) or a chow diet (LAB Diet #5010; calories provided by carbohydrates [58%], fat [13%] and protein [29%])). All food was replaced weekly to avoid contamination. All mice were fasted overnight prior to, glucose metabolism testing, insulin tolerance testing, or terminal harvest (completed between 7–10am). Glucose and insulin tolerance tests were done as previously described[11]. Briefly, following an overnight fast, glucose tolerance levels were determined by injecting mice with 10μL of a 10% dextrose solution per gram of body weight and glucose levels were quantified kinetically at the times shown. For insulin tolerance testing, mice were given 10μL of a 0.15 units/mL solution of insulin (Novolin) per gram of body weight. Hepatic triglyceride deposition, and serum alanine transaminase levels were quantified as previously described[11]. NAFLD activity score (NAS) was determined from H&E staining by a certified pathologist according to standard practice[37]. Total body fat, lean and water mass were determined by nuclear magnetic resonance (Whole Body Composition Analyzer; Echo MRI)[68].

Histology

Oil red O were performed on 5 μm flash frozen tissue sections. Masson's Trichrome and hematoxylin and eosin staining were performed paraffin-embedded tissue blocks. Fibrosis quantification employed the use of an Aperio AT2 Slide Scanner, ImageScope (v. 12.3.1.5011), Color Deconvolution (v9) and Positive Pixel Count (v9; all Leica). Color deconvolution was used to identify the value of the positive stain. This value (0.622712) was subsequently identified in the slides using positive pixel count and percent positive area, which took into account the total number of pixels identified, was quantified.

Flow Cytometry

Single cell suspensions were derived from hepatic homogenate and stained with directly conjugated monoclonal antibodies or isotype controls. Staining for cytokine expression was completed after 4 hours of stimulation with 50 ng/mL Phorbol 12-Myristate 13-acetate (PMA; Promega), 1 μg/mL Ionomycin (Calbiochem) and 10μg/mL Brefeldin A (Gold Bio). Data collection and analysis were done as previously described[11,63]. Briefly, cells were stained with Live/Dead stain (Zombie UV Dye: Biolegend) and with directly-conjugated monoclonal antibodies to CD45-AF700 (104), CD11b-PE (M1/70), F4/80-APCef780 (BM8), Ly6C-Percp (HK1.4), Gr1-FITC (RB6-8C5), NK1.1-PECy7 (PK136), TCRβ-PE (H57-597), CD4-APCef780 (GK1.5), CD8-ef450 (53-6.7), TNF-BV650 (MP6-XT22), IL-17A-Percp (17B7) and IL-17F-PE (18F10) [all antibodies from e-Bioscience]. Flow cytometry data were then collected using a LSR Fortessa (BD) flow cytometer and analyzed using FlowJo X software (vX0.7).

Bacterial Translocation

Liver tissue was homogenized in enriched thioglycollate medium, and subsequently cultured on TSA II/5% sheep blood plates (BD Bioscience).

Intestinal Permeability

1 cm of freshly isolated jejunum was mounted in a U2500 dual Ussing chamber (Warner Instruments). The trans-epithelial resistance and FITC-dextran flux was determined as previously described[69].

Microbiome Analysis

Bacterial DNA was isolated from fecal material when mice arrived at the facility (-2 weeks), before they were placed on diet (0 weeks), and at 12 and 24 weeks after either diet was introduced. Partial 16S rRNA gene sequences were amplified targeting the hypervariable regions v1/v2 using primers 27f (AGAGTTTGATCCTGGCTCAG) and 338r (TGCTGCCTCCCGTAGGAGT). Equimolar amounts of all samples were subjected to sequencing using a MiSeq sequencer from Illumina. Data were then processed using mothur software[70] to determine phylotypes and operational taxonomic units (OTUs) and subjected to statistical analysis. LEfSe analysis was performed using the online tool at https://huttenhower.sph.harvard.edu/galaxy/[71]. For comparison to the human microbiome, individual reads were assigned to taxonomy using the QIIME package[72]. Similarly, raw human 16S sequencing data published by Zhu et al[6] were downloaded from http://metagenomics.anl.gov/linkin.cgi?project=1195 and analyzed using the same QIIME assignment method and analytic pipeline as the mouse 16S read data. Taxonomic data was first analyzed using Mothur software to determine significantly different operational taxa units (OTUs). Similarly, GraphPad Prism (ver 6.07) was used to plot relative species abundance and compare between groups. The Mann-Whitney test was applied to the data to determine statistical significance of observed differences. Between-class principal component analysis was performed using the ade4 package (ver 5.12) in R, something available upon request from corresponding author. Mouse microbiome raw 16S rRNA can be accessed at http://metagenomics.anl.gov/linkin.cgi?project=mgp18319.

Microbiome Manipulation

For antibiotic mediated depletion of Gram-negative bacteria, a cocktail of neomycin and polymixin B sulfate (0.5 and 0.125 mg/mL, respectively) was added to the drinking water after 8 weeks of HFD feeding.

Statistical Analysis

Sample sizes were determined based on preliminary data, which with respect to obesity and NAFLD modeling included weight gain, hepatic triglyceride deposition, immune cell infiltration and hepatocellular damage. Statistical tests were employed for all data sets with similar variance. The test used was dependent on both the number of groups being compared and whether the data were normally distributed. For normally distributed data, Student's *t*-test was used when the comparison was two groups, while a one way ANOVA was employed for 3 or more groups, with Tukey's post hoc test to assess differences between specific groups. For non-parametric data sets the Mann-Whitney test was employed. Statistical analysis was completed using Prism 5a (GraphPad Software, Inc.). All values are represented as means + s.e.m. No animals were excluded from analysis. Studies were not blinded unless otherwise noted above.

Supplementary Material

Refer to Web version on PubMed Central for supplementary material.

Acknowledgments

This work was supported in part by a NIH R01DK099222 and R01DK099222-S1 (to SD), R01DK033201 (to CRK), K12-HD000850 (to SS), NIEHS Grant P30 ES006096 University of Cincinnati Center for Environmental Genomics (associated with DAG), PHS Grant P30 DK078392 Pathology of the Digestive Disease Research Core Center at CCHMC (associated with SD), and German Research Foundation IRTG 1911 (projects A6 and B8 to CS and JR). We would also like to acknowledge Dr. Claire Chougnet (CCHMC, Division of Immunobiology) for providing access to human PBMC samples and Christopher Woods (CCHMC, Division of Pathology and Laboratory Medicine) for technical assistance.

References

1. Ma C, et al. NAFLD causes selective CD4(+) T lymphocyte loss and promotes hepatocarcinogenesis. Nature. 2016; 531:253–257. [PubMed: 26934227]
2. Rinella ME. Will the increased prevalence of nonalcoholic steatohepatitis (NASH) in the age of better hepatitis C virus therapy make NASH the deadlier disease? Hepatology. 2011; 54:1118–1120. [PubMed: 21956705]
3. Tiniakos DG, Vos MB, Brunt EM. Nonalcoholic fatty liver disease: pathology and pathogenesis. Annual review of pathology. 2010; 5:145–171.
4. Rahman K, et al. Loss of Junctional Adhesion Molecule A Promotes Severe Steatohepatitis in Mice on a Diet High in Saturated Fat, Fructose, and Cholesterol. Gastroenterology. 2016; 151:733–746. e712. [PubMed: 27342212]
5. Mehal WZ. The Gordian Knot of dysbiosis, obesity and NAFLD. Nature reviews. Gastroenterology & hepatology. 2013; 10:637–644. [PubMed: 23958600]
6. Zhu L, et al. Characterization of gut microbiomes in nonalcoholic steatohepatitis (NASH) patients: a connection between endogenous alcohol and NASH. Hepatology. 2013; 57:601–609. [PubMed: 23055155]
7. Miele L, et al. Increased intestinal permeability and tight junction alterations in nonalcoholic fatty liver disease. Hepatology. 2009; 49:1877–1887. [PubMed: 19291785]

8. Vespasiani-Gentilucci U, et al. Hepatic toll-like receptor 4 expression is associated with portal inflammation and fibrosis in patients with NAFLD. Liver Int. 2015; 35:569–581. [PubMed: 24649857]
9. Kiziltas S, et al. TLR4 gene polymorphism in patients with nonalcoholic fatty liver disease in comparison to healthy controls. Metab Syndr Relat Disord. 2014; 12:165–170. [PubMed: 24443993]
10. Mills KH. TLR-dependent T cell activation in autoimmunity. Nat Rev Immunol. 2011; 11:807–822. [PubMed: 22094985]
11. Harley IT, et al. IL-17 signaling accelerates the progression of nonalcoholic fatty liver disease in mice. Hepatology. 2014; 59:1830–1839. [PubMed: 24115079]
12. Rau M, et al. Progression from Nonalcoholic Fatty Liver to Nonalcoholic Steatohepatitis Is Marked by a Higher Frequency of Th17 Cells in the Liver and an Increased Th17/Resting Regulatory T Cell Ratio in Peripheral Blood and in the Liver. J Immunol. 2016; 196:97–105. [PubMed: 26621860]
13. Hebbard L, George J. Animal models of nonalcoholic fatty liver disease. Nature reviews. Gastroenterology & hepatology. 2011; 8:35–44. [PubMed: 21119613]
14. Karp CL. Unstressing intemperate models: how cold stress undermines mouse modeling. J Exp Med. 2012; 209:1069–1074. [PubMed: 22665703]
15. Gordon, CJ. Temperature regulation in laboratory rodents. Cambridge University Press; Cambridge England; New York, NY, USA: 1993.
16. Maloney SK, Fuller A, Mitchell D, Gordon C, Overton JM. Translating animal model research: does it matter that our rodents are cold? Physiology (Bethesda). 2014; 29:413–420. [PubMed: 25362635]
17. Stemmer K, et al. Thermoneutral housing is a critical factor for immune function and diet-induced obesity in C57BL/6 nude mice. Int J Obes (Lond). 2015; 39:791–797. [PubMed: 25349057]
18. Bowers SL, Bilbo SD, Dhabhar FS, Nelson RJ. Stressor-specific alterations in corticosterone and immune responses in mice. Brain Behav Immun. 2008; 22:105–113. [PubMed: 17890050]
19. Giles DA, et al. Modulation of ambient temperature promotes inflammation and initiates atherosclerosis in wild type C57BL/6 mice. Mol Metab. 2016; 5:1121–1130. [PubMed: 27818938]
20. Rudaya AY, Steiner AA, Robbins JR, Dragic AS, Romanovsky AA. Thermoregulatory responses to lipopolysaccharide in the mouse: dependence on the dose and ambient temperature. Am J Physiol Regul Integr Comp Physiol. 2005; 289:R1244–1252. [PubMed: 16081879]
21. Moragues V, Pinkerton H. Variation in Morbidity and Mortality of Murine Typhus Infection in Mice with Changes in the Environmental Temperature. J Exp Med. 1944; 79:41–43. [PubMed: 19871351]
22. Foxman EF, et al. Temperature-dependent innate defense against the common cold virus limits viral replication at warm temperature in mouse airway cells. Proc Natl Acad Sci U S A. 2015; 112:827–832. [PubMed: 25561542]
23. Eng JW, et al. Housing temperature-induced stress drives therapeutic resistance in murine tumour models through beta2-adrenergic receptor activation. Nat Commun. 2015; 6:6426. [PubMed: 25756236]
24. Tian XY, et al. Thermoneutral Housing Accelerates Metabolic Inflammation to Potentiate Atherosclerosis but Not Insulin Resistance. Cell Metab. 2016; 23:165–178. [PubMed: 26549485]
25. Athyros VG, et al. Cardiovascular risk across the histological spectrum and the clinical manifestations of non-alcoholic fatty liver disease: An update. World J Gastroenterol. 2015; 21:6820–6834. [PubMed: 26078558]
26. Kox M, et al. Voluntary activation of the sympathetic nervous system and attenuation of the innate immune response in humans. Proc Natl Acad Sci U S A. 2014; 111:7379–7384. [PubMed: 24799686]
27. Hanssen MJ, et al. Short-term cold acclimation improves insulin sensitivity in patients with type 2 diabetes mellitus. Nat Med. 2015; 21:863–865. [PubMed: 26147760]
28. Overton JM. Phenotyping small animals as models for the human metabolic syndrome: thermoneutrality matters. Int J Obes (Lond). 2010; 34(Suppl 2):S53–58. [PubMed: 21151148]

29. Stemmer K, et al. Thermoneutral housing is a critical factor for immune function and diet-induced obesity in C57BL/6 nude mice. Int J Obes (Lond). 2014
30. Swoap SJ, et al. Vagal tone dominates autonomic control of mouse heart rate at thermoneutrality. American journal of physiology. Heart and circulatory physiology. 2008; 294:H1581–1588. [PubMed: 18245567]
31. Emre Y, Nubel T. Uncoupling protein UCP2: when mitochondrial activity meets immunity. FEBS Lett. 2010; 584:1437–1442. [PubMed: 20227410]
32. Bhattacharyya S, Brown DE, Brewer JA, Vogt SK, Muglia LJ. Macrophage glucocorticoid receptors regulate Toll-like receptor 4-mediated inflammatory responses by selective inhibition of p38 MAP kinase. Blood. 2007; 109:4313–4319. [PubMed: 17255352]
33. Izeboud CA, Mocking JA, Monshouwer M, van Miert AS, Witkamp RF. Participation of beta-adrenergic receptors on macrophages in modulation of LPS-induced cytokine release. J Recept Signal Transduct Res. 1999; 19:191–202. [PubMed: 10071758]
34. Emre Y, et al. Mitochondria contribute to LPS-induced MAPK activation via uncoupling protein UCP2 in macrophages. Biochem J. 2007; 402:271–278. [PubMed: 17073824]
35. Wahle M, et al. Beta2-adrenergic receptors mediate the differential effects of catecholamines on cytokine production of PBMC. J Interferon Cytokine Res. 2005; 25:384–394. [PubMed: 16022583]
36. Xu H, et al. Chronic inflammation in fat plays a crucial role in the development of obesity-related insulin resistance. J Clin Invest. 2003; 112:1821–1830. [PubMed: 14679177]
37. Brunt EM, et al. Nonalcoholic fatty liver disease (NAFLD) activity score and the histopathologic diagnosis in NAFLD: distinct clinicopathologic meanings. Hepatology. 2011; 53:810–820. [PubMed: 21319198]
38. Nagaya T, et al. Down-regulation of SREBP-1c is associated with the development of burned-out NASH. J Hepatol. 2010; 53:724–731. [PubMed: 20655124]
39. Rizki G, et al. Mice fed a lipogenic methionine-choline-deficient diet develop hypermetabolism coincident with hepatic suppression of SCD-1. J Lipid Res. 2006; 47:2280–2290. [PubMed: 16829692]
40. Teufel A, et al. Comparison of Gene Expression Patterns Between Mouse Models of Nonalcoholic Fatty Liver Disease and Liver Tissues From Patients. Gastroenterology. 2016; 151:513–525. e510. [PubMed: 27318147]
41. Brown MP, et al. Knowledge-based analysis of microarray gene expression data by using support vector machines. Proc Natl Acad Sci U S A. 2000; 97:262–267. [PubMed: 10618406]
42. Alexander J, Chang GQ, Dourmashkin JT, Leibowitz SF. Distinct phenotypes of obesity-prone AKR/J, DBA2J and C57BL/6J mice compared to control strains. Int J Obes (Lond). 2006; 30:50–59. [PubMed: 16231032]
43. Li L, Chen L, Hu L. Nuclear Factor High-mobility Group Box1 Mediating the Activation of Toll-like Receptor 4 Signaling in Hepatocytes in the Early Stage of Non-alcoholic Fatty Liver Disease in Mice. J Clin Exp Hepatol. 2011; 1:123–124. [PubMed: 25755327]
44. Wieckowska A, et al. Increased hepatic and circulating interleukin-6 levels in human nonalcoholic steatohepatitis. The American journal of gastroenterology. 2008; 103:1372–1379. [PubMed: 18510618]
45. Vandanmagsar B, et al. The NLRP3 inflammasome instigates obesity-induced inflammation and insulin resistance. Nature medicine. 2011; 17:179–188.
46. Langrish CL, et al. IL-23 drives a pathogenic T cell population that induces autoimmune inflammation. J Exp Med. 2005; 201:233–240. [PubMed: 15657292]
47. Ramesh R, et al. Pro-inflammatory human Th17 cells selectively express P-glycoprotein and are refractory to glucocorticoids. J Exp Med. 2014; 211:89–104. [PubMed: 24395888]
48. Sano T, et al. An IL-23R/IL-22 Circuit Regulates Epithelial Serum Amyloid A to Promote Local Effector Th17 Responses. Cell. 2015; 163:381–393. [PubMed: 26411290]
49. Pan JJ, Fallon MB. Gender and racial differences in nonalcoholic fatty liver disease. World J Hepatol. 2014; 6:274–283. [PubMed: 24868321]
50. Kanuri G, Bergheim I. In vitro and in vivo models of non-alcoholic fatty liver disease (NAFLD). Int J Mol Sci. 2013; 14:11963–11980. [PubMed: 23739675]

51. Backhed F, Manchester JK, Semenkovich CF, Gordon JI. Mechanisms underlying the resistance to diet-induced obesity in germ-free mice. Proc Natl Acad Sci U S A. 2007; 104:979–984. [PubMed: 17210919]
52. Puddu A, Sanguineti R, Montecucco F, Viviani GL. Evidence for the gut microbiota short-chain fatty acids as key pathophysiological molecules improving diabetes. Mediators Inflamm. 2014; 2014:162021. [PubMed: 25214711]
53. Inra CN, et al. A perisinusoidal niche for extramedullary haematopoiesis in the spleen. Nature. 2015; 527:466–471. [PubMed: 26570997]
54. Alisi A, et al. Plasma high mobility group box 1 protein reflects fibrosis in pediatric nonalcoholic fatty liver disease. Expert Rev Mol Diagn. 2014; 14:763–771. [PubMed: 24927058]
55. do Nascimento JH, Epifanio M, Soder RB, Baldisserotto M. MRI-diagnosed nonalcoholic fatty liver disease is correlated to insulin resistance in adolescents. Acad Radiol. 2013; 20:1436–1442. [PubMed: 24119357]
56. Sorrentino P, et al. Predicting fibrosis worsening in obese patients with NASH through parenchymal fibronectin, HOMA-IR, and hypertension. Am J Gastroenterol. 2010; 105:336–344. [PubMed: 19861959]
57. Jin W, Dong C. IL-17 cytokines in immunity and inflammation. Emerg Microbes Infect. 2013; 2:e60. [PubMed: 26038490]
58. Meng F, et al. Interleukin-17 signaling in inflammatory, Kupffer cells, and hepatic stellate cells exacerbates liver fibrosis in mice. Gastroenterology. 2012; 143:765–776. e761–763. [PubMed: 22687286]
59. Giles DA, Moreno-Fernandez ME, Divanovic S. IL-17 Axis Driven Inflammation in Non-Alcoholic Fatty Liver Disease Progression. Curr Drug Targets. 2015; 16:1315–1323. [PubMed: 26028039]
60. McKee C, et al. Propranolol, a beta-adrenoceptor antagonist, worsens liver injury in a model of non-alcoholic steatohepatitis. Biochem Biophys Res Commun. 2013; 437:597–602. [PubMed: 23850676]
61. McAlees JW, et al. Distinct Tlr4-expressing cell compartments control neutrophilic and eosinophilic airway inflammation. Mucosal Immunol. 2015; 8:863–873. [PubMed: 25465099]
62. Komiyama Y, et al. IL-17 plays an important role in the development of experimental autoimmune encephalomyelitis. J Immunol. 2006; 177:566–573. [PubMed: 16785554]
63. Giles DA, et al. Regulation of Inflammation by IL-17A and IL-17F Modulates Non-Alcoholic Fatty Liver Disease Pathogenesis. PLoS One. 2016; 11:e0149783. [PubMed: 26895034]
64. Chen J, Bardes EE, Aronow BJ, Jegga AG. ToppGene Suite for gene list enrichment analysis and candidate gene prioritization. Nucleic Acids Res. 2009; 37:W305–311. [PubMed: 19465376]
65. Divanovic S, Trompette A, Ashworth JI, Rao MB, Karp CL. Therapeutic enhancement of protective immunity during experimental leishmaniasis. PLoS Negl Trop Dis. 2011; 5:e1316. [PubMed: 21909452]
66. Finkelman, F., Morris, S., Orekhova, T., Sehy, D. The in vivo cytokine capture assay for measurement of cytokine production in the mouse. In: Coligan …, John E., et al., editors. Current protocols in immunology. Vol. Chapter 6. 2003. p. 28
67. Divanovic S, et al. Negative regulation of Toll-like receptor 4 signaling by the Toll-like receptor homolog RP105. Nat Immunol. 2005; 6:571–578. [PubMed: 15852007]
68. Castaneda TR, et al. Metabolic control by S6 kinases depends on dietary lipids. PLoS One. 2012; 7:e32631. [PubMed: 22412899]
69. Wu D, et al. Interleukin-13 (IL-13)/IL-13 receptor alpha1 (IL-13Ralpha1) signaling regulates intestinal epithelial cystic fibrosis transmembrane conductance regulator channel-dependent Cl- secretion. The Journal of biological chemistry. 2011; 286:13357–13369. [PubMed: 21303908]
70. Schloss PD, et al. Introducing mothur: open-source, platform-independent, community-supported software for describing and comparing microbial communities. Appl Environ Microbiol. 2009; 75:7537–7541. [PubMed: 19801464]
71. Segata N, et al. Metagenomic biomarker discovery and explanation. Genome Biol. 2011; 12:R60. [PubMed: 21702898]

72. Caporaso JG, et al. QIIME allows analysis of high-throughput community sequencing data. Nature methods. 2010; 7:335–336. [PubMed: 20383131]

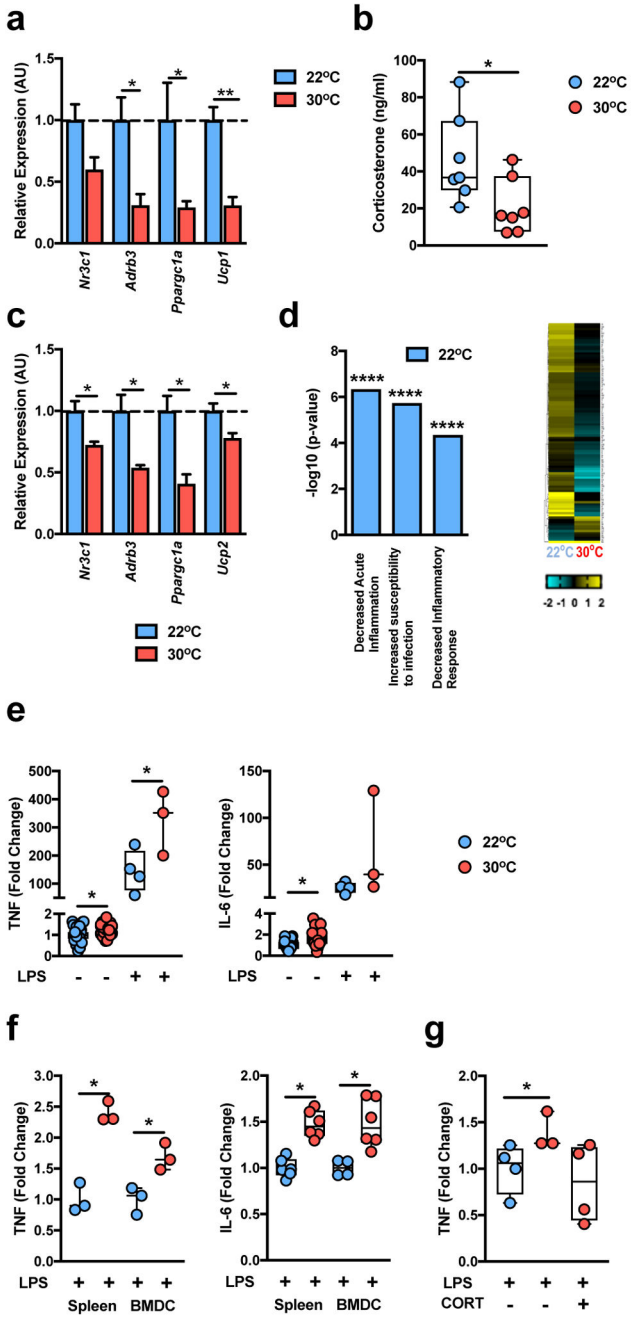

Figure 1.

Thermoneutral housing relieves stress and augments inflammation. (**a–f**) 6 week-old WT C57BL/6 male mice were housed at either standard (T_S; 22°C) or thermoneutral (T_N; 30°C) conditions for a minimum of 3 weeks. (**a**) Expression of the indicated genes in brown adipose tissue ($n = 5$ per group). (**b**) Serum corticosterone levels ($n = 7$ per group). (**c**) Expression of the indicated genes in the spleen ($n = 3$ per group). (**d**) Upregulated gene expression pathways in PBMCs and genes within pathways, determined by RNASeq analysis ($n = 2$ per group). (**e**) Serum TNF and IL-6 level fold change of unstimulated.

T_N-housed (n = 29 per group) mice; LPS-stimulated, T_S housed (n = 4 per group); and T_N-housed (n = 3 per group) mice compared to unstimulated, T_S-housed (n = 31 per group) mice. (**f**) Fold change in splenocyte or BMDC supernatants derived from T_S- or T_N-housed mice for TNF (n = 3 per group) and IL-6 (n = 5 per group). (**g**) Serum fold change for TNF in LPS-treated, T_N-housed (n = 3 per group) and T_N-housed mice also treated with 100mg/L corticosterone in drinking water (n = 4 per group) compared to LPS-treated, T_S-housed mice (n = 4 per group). For bar graphs, data represents mean + s.e.m. (**a–c** and **g**) A single experiment. (**e**) Samples represent combined data of 4 individual experiments. (**f**) A representative of 2 individual experiments. *P < 0.05, **P < 0.01, ***P < 0.001, ****P < 0.0001. (**a–c** and **e–f**) Student's t-test. (**g**) One way ANOVA with *post hoc* Tukey's test.

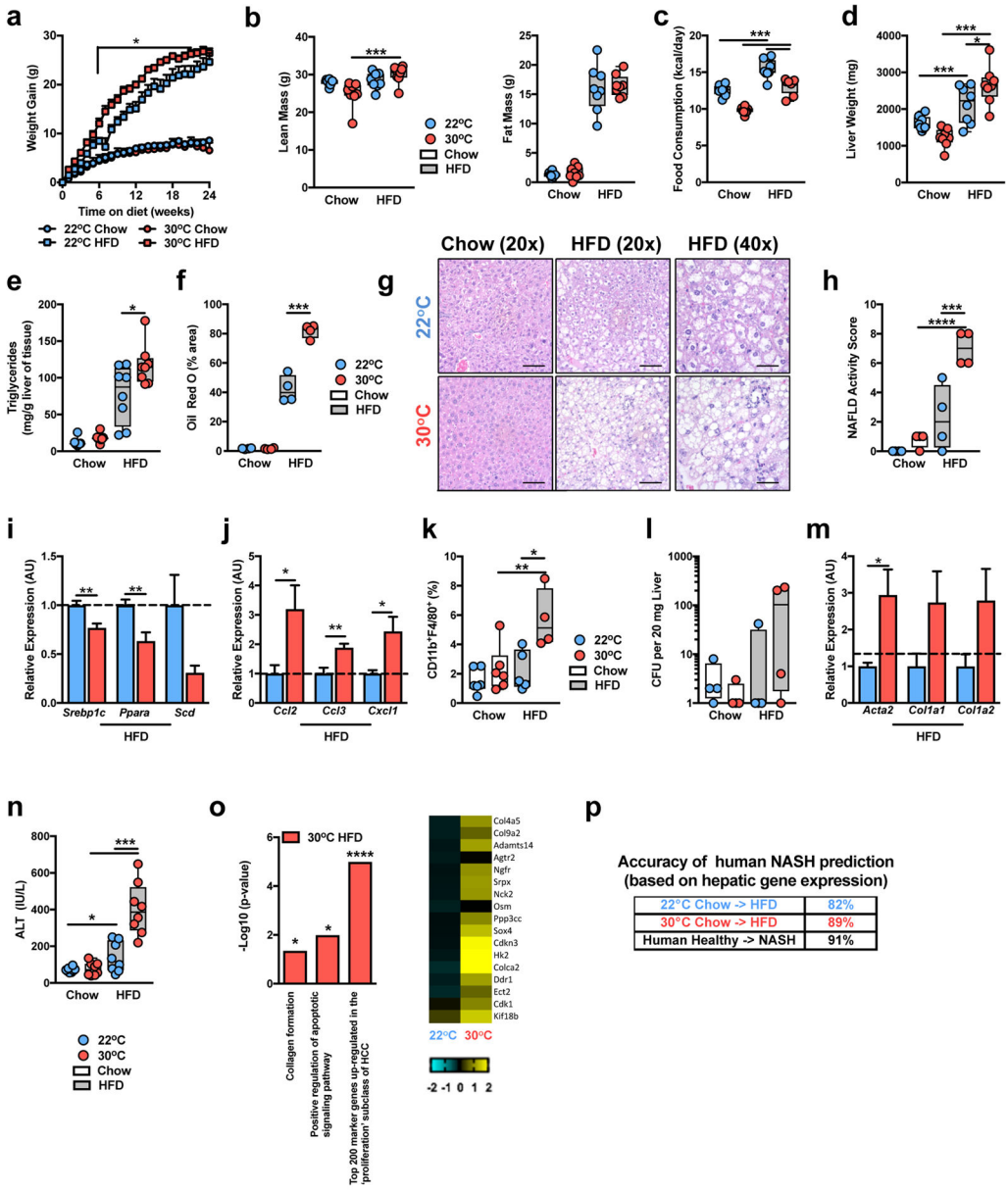

Figure 2.

Thermoneutral housing exacerbates HFD-driven NAFLD pathogenesis. (**a–o**) 6 week-old WT C57BL/6 male mice were housed at T_S (22°C) or T_N (30°C) for 24 weeks and fed a chow or HFD. (**a**) Weight gain. (**b**) Total body lean and fat mass. (**c**) Daily caloric intake. (**d**) Liver weight. (**e**) Hepatic triglyceride levels (**a-e**; *n* = 8 per group). (**f**) Oil red O staining, percent area positive for lipid accumulation. (**g**) Representative liver histology (*n* = 4 per group) by H&E staining at 20x and 40x magnification. Scale bars, 100μm (left and middle) and 50μm (right). (**h**) NAFLD activity score. (**i**) Expression of the indicated lipid mediator genes in the liver. (**j**) Expression of the indicated chemokine genes in the liver. (**k**) Percent of hepatic $CD11b^+F4/80^+$ immune cells. (**l**) Colony forming units (CFU) of aerobic bacteria cultured from liver homogenate. (**m**) Expression of the indicated fibrosis marker genes in the liver (**f–m**; *n* = 4 per group). (**n**) Serum alanine transaminase (ALT) levels (*n* = 8 per group).

(**o**) Upregulated gene expression pathways, and genes within pathways, determined by RNASeq analysis of livers from HFD-fed mice ($n = 2$ per group). (**p**) Predictability of human NASH based on simple machine vector learning technique. Blue denotes T_S (22°C); Red denotes T_N (30°C). Data represents mean + s.e.m. (**a–n**) A representative of 5 individual experiments. (**o** and **p**) A single experiment. *$P < 0.05$, **$P < 0.01$, ***$P < 0.001$, ****$P < 0.0001$. (**a–f**, **h**, **k**, **l** and **n**) One way ANOVA with *post hoc* Tukey's test. (**i**, **j** and **m**) Student's *t*-test.

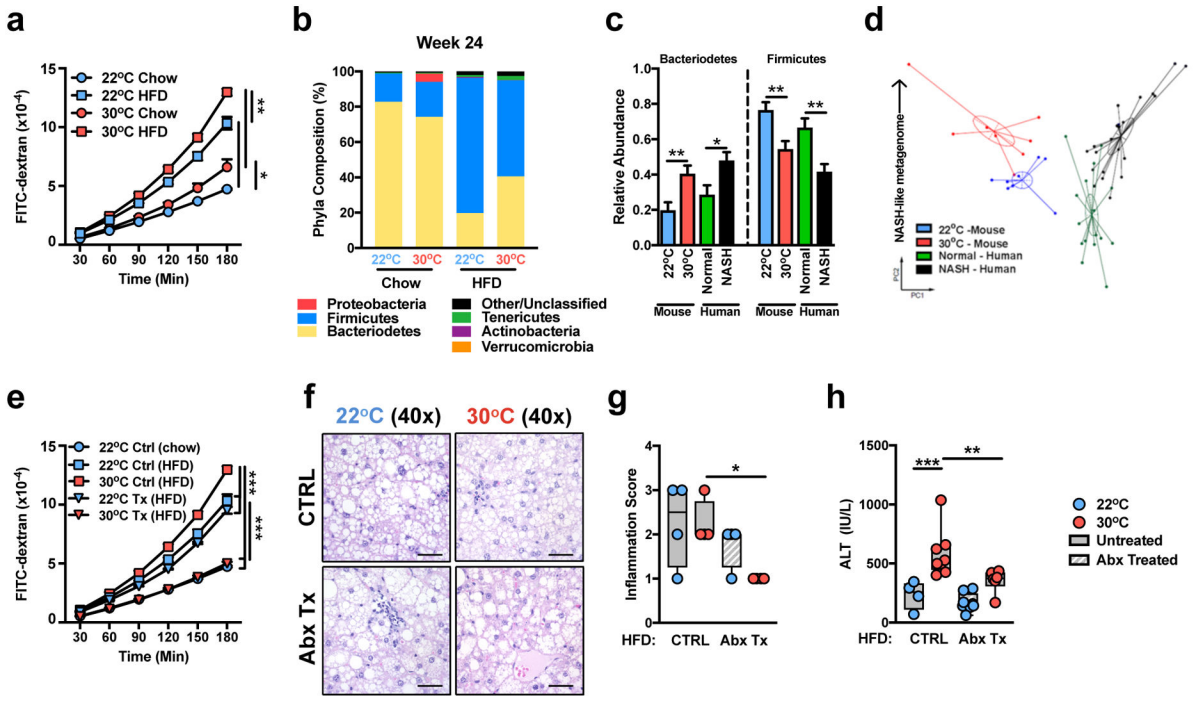

Figure 3.

Thermoneutral housing is associated with augmented intestinal permeability and dysbiosis of the microbiome. (**a–c**) 6 week-old WT C57BL/6 male mice were housed at T_S (22°C) or T_N (30°C) for 24 weeks and fed a chow or HFD. (**a**) Flow of FITC labelled dextran through the intestine ($n = 4$ per group). (**b**) Phyla level differences of T_S and T_N mice after 24 weeks HFD ($n = 8$ per group). (**c**,**d**) Relative phyla abundance and principle coordinate analysis in mice housed at T_S ($n = 8$ per group) or T_N ($n = 8$ per group) and either healthy, lean humans ($n = 16$ per group) or NASH patients ($n = 22$ per group) described previously. (**e–h**) 6 week-old WT C57BL/6 male mice were housed at T_S (22°C) or T_N (30°C) and fed a HFD. After 8 weeks of HFD, mice were mock-treated (Ctrl) or treated with antibiotics (Tx) supplied in drinking water in addition to HFD exposure for additional 16 weeks. (**e**) Flow of FITC labelled dextran through the intestine of control 22°C chow, HFD and 30°C HFD ($n = 4$ per group) and treated 22°C and 30°C HFD ($n = 3$ per group) fed mice. (**f**) Representative liver histology ($n = 4$ per group) by H&E staining. Scale bars, 50μm. (**g**) Inflammation score per NAS criteria ($n = 4$ per group). (**h**) Serum ALT levels ($n = 8$ per group). For bar graphs, data represents mean + s.e.m. (**a**) A representative of 2 individual experiments. (**b–h**) A single experiment. $*P < 0.05$, $**P < 0.01$, $***P < 0.001$, $****P < 0.0001$. (**a**, **e**, **g** and **h**) One way ANOVA with *post hoc* Tukey's test. (**c**) Mann-Whitney test.

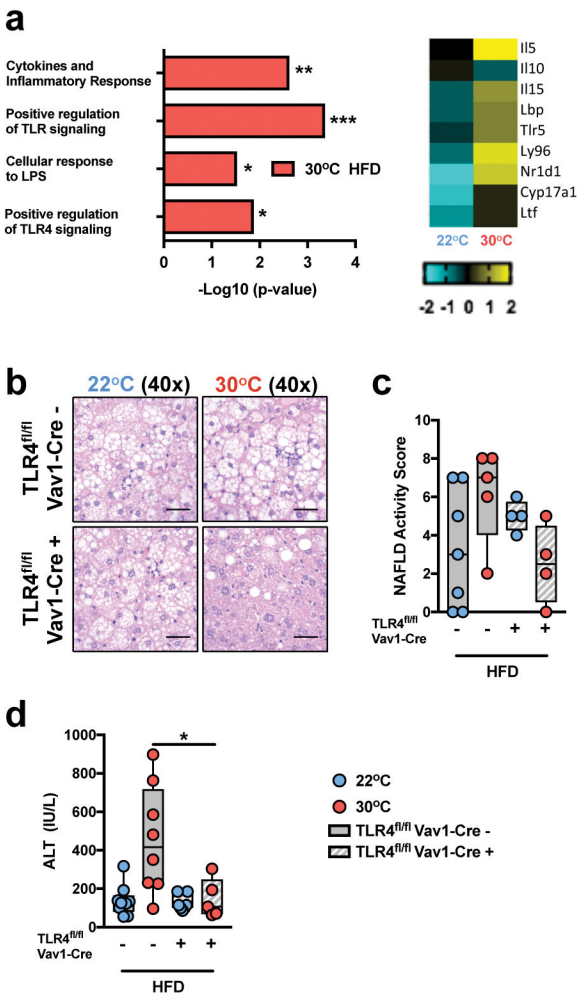

Figure 4.

Thermoneutral housing-driven modulation of hematopoietic TLR4 signaling regulates NAFLD progression. (**a**) 6 week-old WT C57BL/6 male mice were housed at T_S (22°C) or T_N (30°C) conditions for 2 weeks prior to initiation of 8 weeks of HFD. Upregulated gene expression pathways, and genes within pathways, determined by RNASeq analysis ($n = 2$ per group). (**b–d**) 6 week-old TLR4$^{fl/fl}$Vav1-Cre^{+} and control TLR4$^{fl/fl}$Vav1-Cre^{-} mice on a C57BL/6 background were housed at T_S (22°C) or T_N (30°C) for 24 weeks and fed a chow or HFD. (**b**) Representative liver histology by H&E staining at 40x magnification of TLR4$^{fl/fl}$Vav1-Cre^{-} mice housed at 22°C ($n = 3$ per group) and 30°C ($n = 5$ per group) compared to TLR4$^{fl/fl}$Vav1-Cre^{+} mice housed at 22°C ($n = 4$ per group) and 30°C ($n = 4$ per group). Scale bars, 50μm. (**c**) NAFLD activity score as determined by histology. (**d**) Serum ALT levels of TLR4$^{fl/fl}$Vav1-Cre^{-} mice housed at 22°C ($n = 9$ per group) and 30°C ($n = 8$ per group) compared to TLR4$^{fl/fl}$Vav1-Cre^{+} mice housed at 22°C ($n = 7$ per group) and 30°C ($n = 5$ per group). Blue denotes T_S (22°C); Red denotes T_N (30°C). (**a**) A single experiment. (**c–d**) A representative of 2 independent experiments. *$P < 0.05$, **$P < 0.01$, ***$P < 0.001$, ****$P < 0.0001$. (**c–d**) One way ANOVA with *post hoc* Tukey's test.

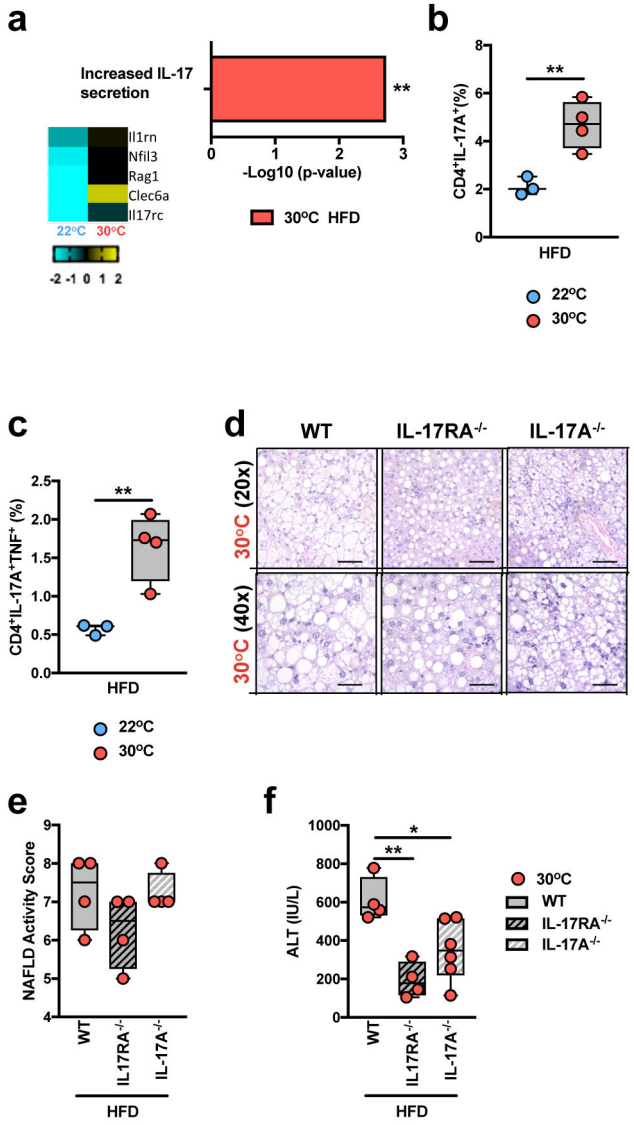

Figure 5.

Thermoneutral housing is associated with pathogenic upregulation of the IL-17 axis. (**a**) 6 week-old WT C57BL/6 male mice were housed at T_S (22°C) or T_N (30°C) conditions for 2 weeks prior to initiation of 8 weeks of HFD feeding. Upregulated gene expression pathway, and genes within pathway, determined by RNASeq analysis (n = 2 per group). (**b–c**) 6 week-old WT C57BL/6 male mice housed at T_S (22°C; n = 3 per group) or T_N (30°C; n = 4 per group) for 24 weeks and fed a HFD. (**b**) Percent of $TCR\beta^+CD4^+IL\text{-}17A^+$ hepatic infiltrating immune cells. (**c**) Percent of $TCR\beta^+CD4^+IL\text{-}17A^+TNF^+$ hepatic infiltrating immune cells. (**d–f**) 6 week-old WT (n = 5 per group), $IL\text{-}17RA^{-/-}$ (n = 4 per group) and $IL\text{-}17A^{-/-}$ (n = 6 per group) male mice, all on C57BL/6 background, were housed at T_N (30°C) conditions for 2 weeks prior to initiation of 24 weeks of HFD feeding. (**d**) Representative liver histology of WT (n = 5 per group), $IL\text{-}17RA^{-/-}$ (n = 4 per group) and $IL\text{-}17A^{-/-}$ (n = 6 per group) mice, by H&E staining at 20x and 40x magnification. Scale bars, 100μm (top) and 50μm (bottom). (**e**) NAFLD activity score. (**f**) serum ALT levels. (**a**) A single experiment. (**b–f**) A

representative of 3 individual experiments. *$P < 0.05$, **$P < 0.01$, ***$P < 0.001$, ****$P < 0.0001$. (**b**–**c**) Student's *t*-test. (**e**–**f**) One way ANOVA with *post hoc* Tukey's test.

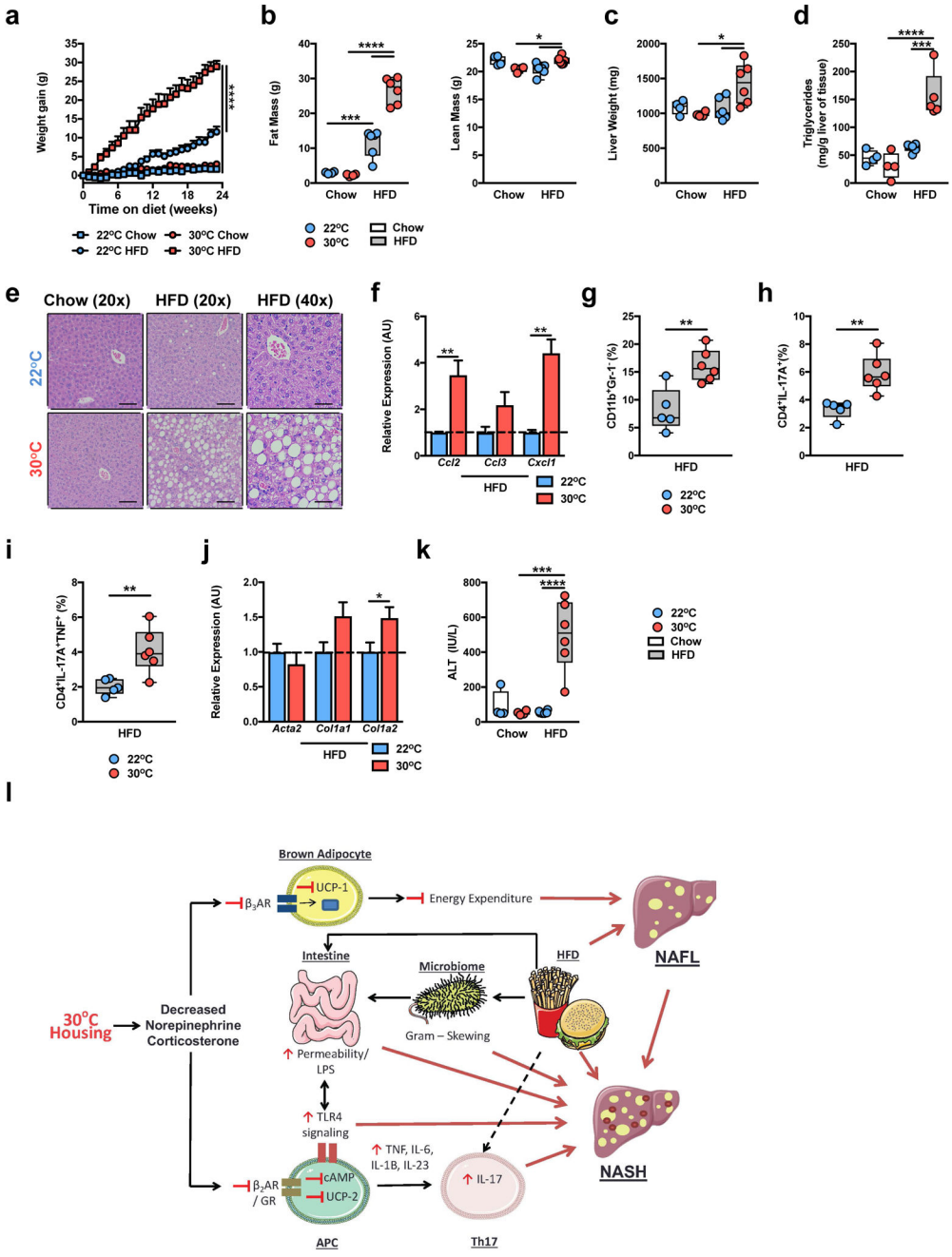

Figure 6.

Thermoneutral housing removes the barrier to modeling obesity and NAFLD in female mice. (**a–k**) 6 week-old WT C57BL/6 female mice housed at T_S (22°C) fed chow (n = 4 per group) or HFD (n = 6 per group) or housed at T_N (30°C) and fed chow (n = 4 per group) or HFD (n = 6 per group) for 24 weeks. (**a**) Weight gain. (**b**) Total body fat mass and lean mass. (**c**) Liver weight. (**d**) Hepatic triglyceride levels. (**e**) Representative liver histology (n = 4 per group) by H&E staining at 20x and 40x magnification. Scale bars, 100μm (left and middle) and 50μm (right). (**f**) Expression of the indicated chemokine genes in the liver of HFD fed

mice. (**g**) Percent of hepatic infiltrating $CD11b^{+}GR\text{-}1^{-}$ immune cells in HFD fed mice. (**h**) Percent of hepatic infiltrating Th17 cells in total hepatic immune cell infiltrate in HFD fed mice. (**i**) Percent of hepatic infiltrating Th17 cells also producing TNF in total hepatic immune cell infiltrate in HFD fed mice. (**j**) Expression of the indicated fibrosis marker genes in the liver in HFD fed mice. (**k**) Serum ALT levels in chow and HFD fed mice. (**l**) Schematic diagram depicting the role of T_N housing in promoting exacerbated NAFLD pathogenesis during HFD feeding where red lines represent factors associated with exacerbated NAFLD at T_N (APC – Antigen presenting cells; NAFL – Nonalcoholic Fatty Liver). This schematic, in part, is composed by available artwork (http://www.servier.com/Powerpoint-image-bank), per licensing agreement (https://creativecommons.org/licenses/by/3.0/legalcode). For bar graphs, data represents mean + s.e.m. (**a–k**) A representative of 3 individual experiments. $*P < 0.05$, $**P < 0.01$, $***P < 0.001$, $****P < 0.0001$. (**a–d** and **k**) one way ANOVA with *post hoc* Tukey's test. (**f–j**) Student's *t*-test.